**Annales
Geophysicae**

Statistical signature of active D-region HF heating in IRIS riometer data from 1994–2004

A. Kero[1], C.-F. Enell[1], Th. Ulich[1], E. Turunen[1], M. T. Rietveld[2], and F. H. Honary[3]

[1]Sodankylä Geophysical Observatory, University of Oulu, Sodankylä, Finland
[2]EISCAT Scientific Association, Ramfjordmoen, Norway
[3]Dept. of Communication Systems, Lancaster University, UK

Abstract. In this paper we study the effect of artificial HF heating on cosmic radio noise absorption in the D-region ionosphere. The effect has earlier been studied theoretically in idealised cases and without experimental verification. Here we present a 3-dimensional modelling of the effect, taking into account the directivity patterns of the vertical beam of the EISCAT Heater at Tromsø, Norway, and the intersecting beam of the IRIS imaging riometer at Kilpisjärvi, Finland. The heater-induced enhancement of cosmic radio noise absorption at the IRIS frequency (38.2 MHz) is estimated to be between 0.02 dB and 0.05 dB in the most representative model cases.

However, a statistical study of IRIS data from a selected set of heating experiments carried out during the years 1994–2004 shows that the median effect is between 0.002 dB and 0.004 dB, i.e. an order of magnitude less than theoretically predicted. This indicates that the actual HF heating effect at D-region altitudes is substantially overestimated by the present theory.

Keywords. Ionosphere (Active experiments; Instruments and techniques) – Electromagnetics (Wave propagation)

1 Introduction

Radio wave absorption is known to take place in the ionospheric D-region through collisions of electrons, which are accelerated by the electric field of the radio wave, with neutral atoms and molecules. Radio wave absorption provides experimental access to the D-region, the probing of which is otherwise difficult. A widely used method is monitoring of cosmic background radio noise with riometers (relative ionospheric opacity meters). Imaging riometers, such

as the Imaging Riometer for Ionospheric Studies (IRIS) system (Detrick and Rosenberg, 1990; Browne et al., 1995) at Kilpisjärvi, Finland (69.05° N, 20.79° E), use narrow-beam formation by phased-array antennas in order to monitor spatial structures of the ionosphere (see Fig. 1).

The absorption of radio waves also makes it possible to heat the ionospheric electron gas using high-power HF transmitters. The heating facility of the European Incoherent Scatter Scientific Association (EISCAT) at Tromsø, Norway (69.6° N, 19.2° E) has been designed for this purpose (see Rietveld et al., 1992). According to earlier modelling work (Belova et al., 1995; Kero et al., 2000) the facility, which has an effective radiated power (ERP) of up to 1.2 GW, is capable of increasing the electron temperature by a factor of ten at a maximum. However, the modelled maximal effect has not been verified by any observations. The lack of EISCAT radar verification is due to the electron densities generally being below the detection limit at the altitude of the maximal heating effect.

In contrast to radar measurements, passive monitoring of any HF radio waves penetrating through the heated volume can be used as a diagnostic technique. This is possible because the increased electron temperature raises the electron-neutral collision frequency, and therefore decreases the transparency of the plasma. This additional absorption can be supposed to take place and disappear practically immediately, in timescales of milliseconds, when the heater is turned on and off (Rietveld et al., 1986). To a lesser extent, the transparency may also change through electron temperature dependent chemistry (formation of negative ions) during the heating periods (Enell et al., 2005), but the magnitude of this effect is marginal and its time constant is several seconds to minutes. Thus the effect on cosmic radio noise intensity seen in the riometer beam overlapping the heated volume is expected to be a step function of a certain magnitude added to the natural variations of the transparency. Pashin et al. (2003) and Enell et al. (2005) have estimated the magnitude of the

---

Correspondence to: A. Kero
(antti.kero@sgo.fi)
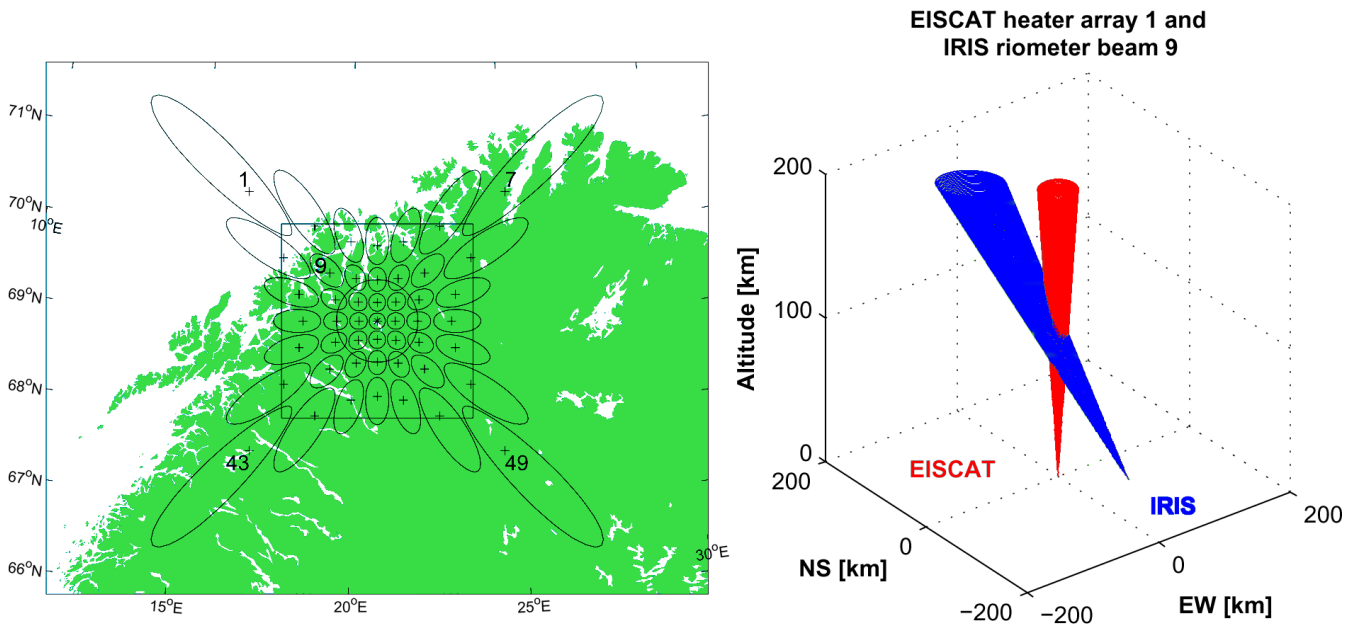
Fig. 1. Left panel: Kilpisjärvi IRIS riometer beam projections at 90 km on a map of northern Scandinavia. Right panel: Intersection of the main lobe of EISCAT heater antenna field 1 and IRIS beam 9.

effect to be several tenths of a dB, provided that the geometry is ideal and that the modelled electron temperature increase is correct.

A competing increase in the noise intensity observed by the riometer is possible because of scintillations produced by heater-enhanced refractive indices of the F region (Honary et al., 2000). However, as Fig. 1 shows, beam number 9 of the Kilpisjärvi IRIS riometer crosses the vertical main lobe of the EISCAT heater at D-region altitudes and should not be affected by any F-region heating effects. This study is dedicated to finding the D-region heating effect and its magnitude, both by modelling and by statistical analysis of IRIS beam 9 data as contrasted to the other IRIS beams not overlapping the heated volume.

2 Modelling

2.1 Radio wave absorption

Radio wave propagation in a collisional magnetised plasma is described by the refractive index n, whose imaginary part $\Im(n) < 0$ determines the attenuation of the wave. The intensity I of the wave along a path r is

$$I(r) = I_0 \exp\left(\frac{2\omega}{c} \int_0^r \Im(n(r)) \, dr\right) \quad (1)$$

Here ω is the radio-wave angular frequency, I_0 the intensity without absorption and c the speed of light. The generalised Appleton dispersion theory given by Sen and Wyller (1960)

is used to calculate the refractive indices n_o and n_x for the ordinary (○) and extraordinary (×) modes of polarisation. The refractive indices are functions of the electron density N_e, the external magnetic field $\boldsymbol{B}$ and the electron-neutral collision frequency ν_{en}. A sum of electron temperature dependent rates of momentum transfer to N_2, O_2 and O, listed by Banks and Kockarts (1973), is used for ν_{en} whereas the pure magnetic dipole approximation is used for $\boldsymbol{B}$.

In the model Eq. (1) is calculated numerically as $I(r) = I_0 D(r)$, where the decay D due to absorption is approximated by a sum over steps Δr as

$$D(r) = \exp\left(\frac{2\omega}{c} \sum_r \Im(n_r) \Delta r\right) \quad (2)$$

In this paper both the absorption of the heater radio wave and of the cosmic radio noise are calculated using Eq. (2).

2.2 Heating model

The intensity of a radio wave, emitted by the heater antenna field, along a ray path r is determined by Eq. (1), where the unabsorbed intensity is given by transmitter power P and antenna gain G in the ray direction:

$$I_0 = \frac{PG}{4\pi r^2} \quad (3)$$

Heater radiation patterns (in dB scale) for antenna fields 1 and 2 of the Eiscat heater are illustrated in Fig. 2, upper right panel.
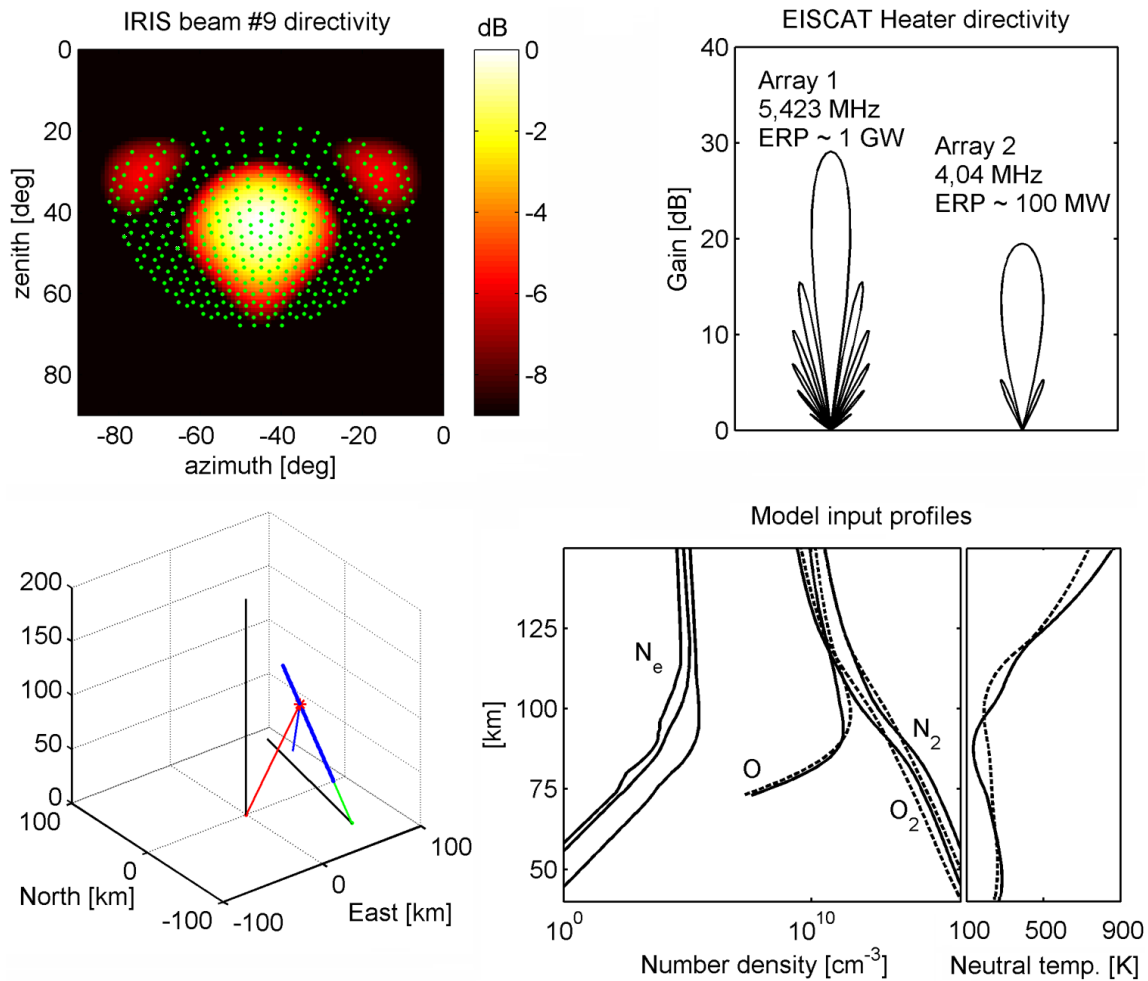
Fig. 2. Upper left panel: Beam directivity of Kilpisjärvi IRIS beam 9 and the 401 ray paths used in modelling the absorption (found using triangular tesselation with equally spaced barycentres). Upper right panel: Antenna beam directivities for antenna fields 1 and 2 of the Eiscat heater. Lower left panel: Ray paths used in the modelling of the heater effect. Black lines are centre lines of heater beam and IRIS beam 9. The green line shows one of the 401 barycentre directions along which the model is run in 1-km steps (blue points). The red line is the heater line-of-sight direction for one of these model points. Lower right panel: Profiles of electron density (Friedrich et al., 2004), atmospheric neutral components and temperature (MSISE-90) for the modelling cases.

Consider now the energy transfer from the radio wave to the electron gas due to absorption. According to Eq. (1) the absorbed power per volume is

$$Q = \frac{2\omega}{c}\Im(n(r))I(r). \tag{4}$$

Electron energy loss occurs through collisions with neutrals. In the model, the electron energy loss rate L is the sum of the rates of rotational and vibrational excitation of O_2 and N_2 given by Pavlov (1998a,b) and the rates due to collisions with atomic oxygen according to Stubbe and Varnum (1972). All loss rates are functions of prevailing electron temperature T_e. Note that also Q depends on the electron temperature, because the imaginary part of the refractive index, $\Im(n)$, depends on the electron-neutral collision frequency ν_{en}, which

is a function of T_e. Hence, the electron temperature is determined by

$$kQ(T_e) = L(T_e) \tag{5}$$

under thermal equilibrium. We introduce a scaling factor k, which is typically set to unity assuming that the absorbed energy is entirely transferred to electron thermal energy and that all loss processes are known. The use of this constant scaling factor is a zeroth-order parameterisation of possible unknown electron energy gain and loss processes, or errors in input parameters such as overestimated transmitter power. In reality the scaling factor can be a function of electron temperature. The sensitivity of the model for values $k<1$ is studied in Sect. 2.5.

The electron temperature along the ray path in 1 km stratified layers is modelled using the routine described by Kero et al. (2000) which follows Belova et al. (1995).

First, the intensity of the wave is calculated on a ray path at each altitude h using Eqs. (2) and (3). The equilibrium electron temperature $T_e(h)$ that fulfils Eq. (5) is solved for within 1 K tolerance. Thereafter the refractive index of the layer must be recalculated for the new electron-neutral collision frequency determined by the increased electron temperature $T_e(h)$. The intensity penetrating into next layer, and its electron temperature, can be calculated in the same fashion. This procedure is continued until a desired altitude.

In our application, the electron temperature is modelled for each 1-km step along an IRIS riometer ray through the ionosphere (see Fig. 2, lower left panel, crossing of blue and red lines). The electron temperatures thus obtained are used in the following calculations of cosmic radio noise absorption.

2.3 Cosmic radio noise absorption model

The cosmic radio noise absorption $A_r(t_{sid})$ detected by a riometer is a measure of the noise power $P(t_{sid})$ compared with a certain reference value called the quiet-day power $P_Q(t_{sid})$, so that $A_r = 10 \log \left(P(t_{sid})/P_Q(t_{sid}) \right)$. The sidereal time t_{sid} is used because the power is a function of the number of distant cosmic radio sources seen by the riometer beam.

We assume that the extraionospheric cosmic radio noise is an isotropic energy flux of randomly polarised waves, so that statistically the radio noise intensity (power per unit solid angle) is independent of direction and both modes of propagation have equal intensity ($I_{0o} = I_{0x}$).

Let the intensity given by Eq. (1) represent a small solid angle element around the ray. The total power detected by the riometer is then an integral of the intensity over all solid angles weighted by the directivity function w_D of the instrument:

$$P = \int_{\Omega} w_D(\Omega)(I_o + I_x)\, d\Omega. \qquad (6)$$

In the model, the integral is solved numerically as a mean of calculated intensities in the barycentres of N triangular tesselations, weighted both by the solid angle $\Delta\Omega_i$ of each triangle, and by the instrument directivity function w_{Di} in the barycentre direction

$$P = \frac{\sum\limits_{i=1}^{N}(I_o + I_x)\Delta\Omega_i w_{Di}}{\sum\limits_{i=1}^{N} \Delta\Omega_i w_{Di}} \qquad (7)$$

The absorption difference between heated (H) and background (BG) ionosphere is modelled based on Eqs. (2) and (7) as follows:

$$\Delta A_r = A_H - A_{BG} = 10\log\left(P_H/P_{BG}\right) \qquad (8)$$

$$= 10\log\left(\frac{\sum\limits_{i=1}^{N} \Delta\Omega_i w_{Di}\,(D_{oHi} + D_{xHi})}{\sum\limits_{i=1}^{N} \Delta\Omega_i w_{Di}\,(D_{oBGi} + D_{xBGi})} \right)$$

$$D_{MCi} = \exp\left(\sum_r \Im(n_{MCir})\Delta r \right)$$

where D_{MCi} is calculated for each tesselation direction i and all combinations of mode M (x or $\circ$) and case C (H or BG). The corresponding refractive indices for the heated case, n_{oHir} and n_{xHir}, are calculated using the electron temperatures modelled as in Sect. 2.2, whereas for the background refractive indices n_{oBGir} and n_{xBGir} the electron temperature is set equal to the neutral temperature. The refractive indices are calculated at the frequency of the Kilpisjärvi IRIS riometer (38.2 MHz). Note that ΔA_r, as a relative quantity, does not depend on the isotropic source intensity I_0. The directivity function w_D of Kilpisjärvi IRIS beam 9 and the equally spaced triangular tesselation barycentres (N=401) are illustrated in the upper left panel of Fig. 2.

2.4 Model results

The absorption differences ΔA_r were modelled with the following selected sets of input parameters, shown in Fig. 2, lower right panel:

- 3 electron density profiles (low, medium and high) obtained from a statistical model developed by Friedrich et al. (2004), representing night-time riometer absorptions of 0.1, 0.3 and 3 dB; logarithmic extrapolation is used below 70 km

- 2 neutral atmosphere density and temperature profiles (winter and summer) from the MSISE-90 model (Hedin, 1991)

- Power and gain of the EISCAT heater antenna fields 1 and 2 with their lowest usually used frequencies (field 1: 4.04 MHz and field 2: 5.423 MHz) for vertical heater beams

- 2 Heater wave polarisations: $\circ$- and x-mode

The model was run for all combinations of input parameters above (24 cases) in order to cover most of the variety of conditions and chosen parameters corresponding to the experiments carried out at the EISCAT Heater Facility in 1994–2004. The number of tesselation points N=401 and the model scaling factor k=1 were the same in all the cases. The specified nominal maximum output power of the heater is 12×100 kW, using all 12 power amplifiers. In the following modelling we assume, as a conservative estimate, that on average each power amplifier outputs 85 kW.
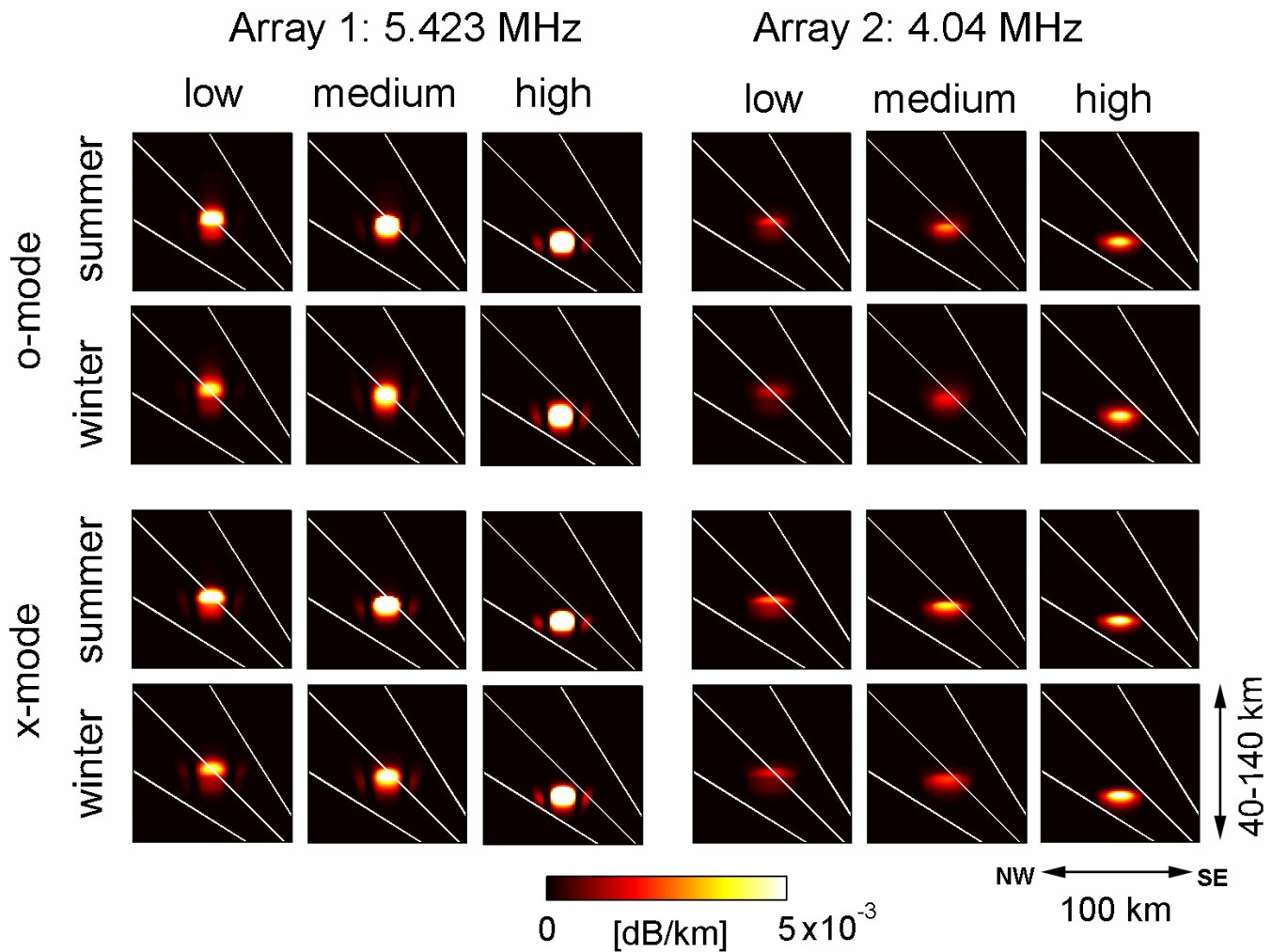
Fig. 3. Modelling of the increase in differential riometer absorption for 24 type cases of heating. The plots show vertical slices through the model volume in the NW-SE direction.

The modelled heating effect on the absorption of cosmic radio noise is illustrated in Fig. 3 for all 24 cases. In the 2-dimensional intersections shown, the effects of antenna field selection and electron density are clearly visible. Field 1 produces an intense narrow effect including also faint signatures of the first sidelobes, while field 2 gives a broad but faint effect. The higher the electron density is, the stronger is the effect, although that is partially compensated by a slight downshift from the IRIS beam center. Variations between polarisation modes and seasons are not that clear.

The integrated cosmic radio wave absorption differences ΔA_r, calculated according to Eq. (8), are shown in Fig. 4. The absorption difference modelled for IRIS beam 9 is, in all the cases, larger than 0.01 dB. The most significant parameter is the antenna gain, which depends on the selection of heater antenna field: in average, field 2 produces only half the corresponding effect of field 1 in dB scale. An increase of the

effect as a function of electron density is also clearly visible in all cases. Some minor-scale differences are found between seasons: summer atmosphere yields higher effects, except in the high electron density case with antenna field 2. The more efficiently absorbed x-mode seems to produce slightly higher effects in most of the cases, except for the combination of high electron density and field 1. There the x-mode effect is shifted too far downwards compared with the less absorbed o-mode, which penetrates closer to the center of the IRIS beam.

2.5 Model sensitivity tests

In order to study the accuracy of the model, tests for model sensitivity to changes of some parameters are shown in Fig. 5.

The upper left panel illustrates how the absorption difference estimates of all 24 modelled cases converge as a
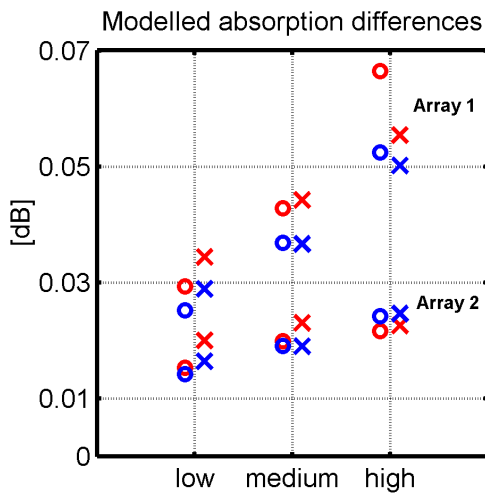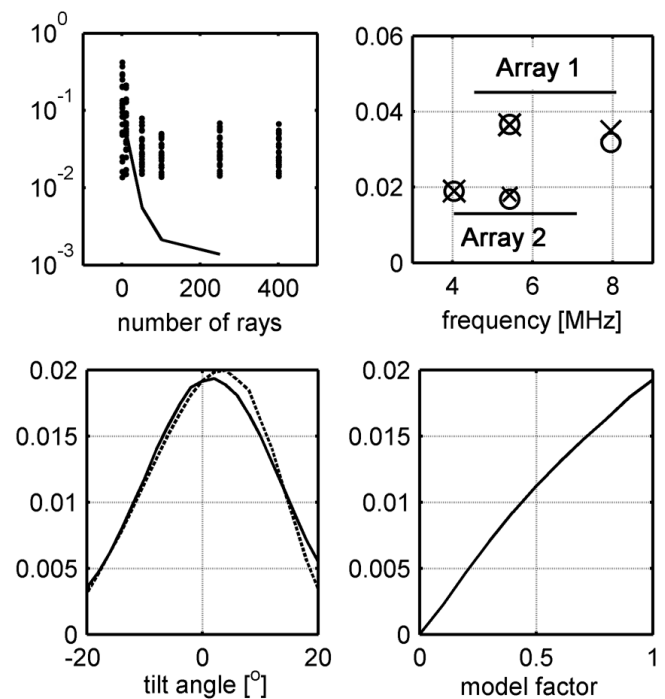
Fig. 4. Spatially integrated absorption differences for all combinations of antenna fields (Array 1 and Array 2), modes (x and ○), season (red=summer, blue=winter) and electron density (low, medium, high); in total 24 cases.

function of the number of tesselations (N) used. The deviation between N=401 and N=250 is 0.1% in average and 0.3% at a maximum. Hence, the used N=401 describes the geometry of the experminent well and, in fact, results obtained with N=250 can as well be considered correct, if there is a need for saving calculation time.

In the modellings shown in Fig. 4, only the lowest recommended frequency was used for each antenna field (Field 1: 5.423 MHz, Field 2: 4.04 MHz). In the current model, directivity patterns are also available for one higher frequency of each antenna field. Modelling using these higher frequencies (Field 1: 7.953 MHz, Field 2: 5.423 MHz) was done for both ○- and x-mode under winter-time medium-N_e conditions. The results are compared with the corresponding lower-frequency cases in Fig. 5, upper right panel. Although the higher frequencies produce slightly smaller effects, the difference is less than 0.002 dB/MHz for both antenna fields. Hence, the variation due to different heater frequencies can be expected to be neglible, especially when taking into account the fact that the lowest frequencies are more often used in the EISCAT heating experiments (see Table 1), in contrast to the seldom used highest frequencies.

Beam 9 of the Kilpisjärvi IRIS riometer is pointing in the direction from SE towards NW ($-45°$ from the riometer), which is close to perfectly matching the vertical EISCAT Heater beam (the azimuth angle difference is only 1.5 degrees). Figure 3 shows that also the zenith angle of IRIS beam 9 is close to optimal, providing the maximum heating effect well inside the beam according to modelling. The lower left panel of Fig. 5 illustrates the importance of the accuracy of the IRIS beam directions by showing the modelled absorption difference as a function of IRIS azimuth and
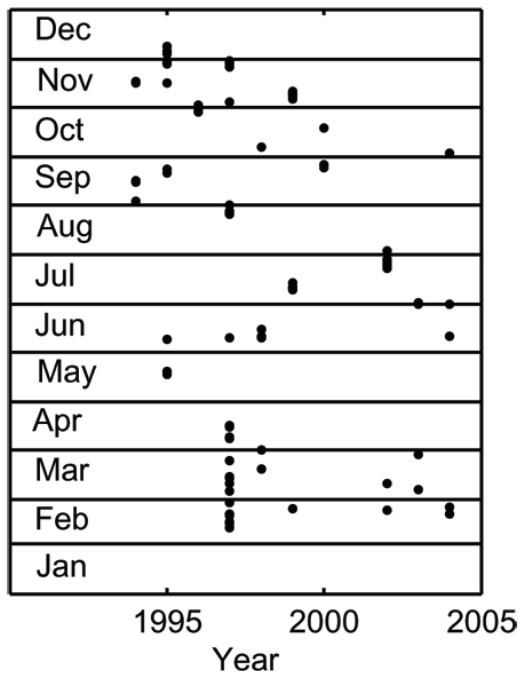

Fig. 5. Model sensitivity tests. All panels show modelled absorption differences in dB. Upper left panel: Integrated absorption difference vs. number of tesselations used in the 3-D model (points) and deviation from the 401-point case (solid line). Upper right panel: The effect of heater frequency calculated for the winter-time medium electron density case and both ○- and x-modes. Solid lines represent the full frequency ranges of the two antenna fields. Lower left panel: The effect of possible IRIS beam horizontal (solid line) and vertical (dashed line) misalignment. Lower right panel: The effect of the model production/loss scaling factor k explained in Sect. 2.2.

zenith angle tilts. Our estimate for the accuracy of the IRIS beam direction is ± 5 degrees, which corresponds roughly to a $\pm 10\%$ error in the modelled absorption difference, at a maximum.

The lower right panel of Fig. 5 shows the modelled absorption difference as a function of the model scaling factor k. The relation between absorption difference and k is almost linear, which makes it easy to scale the modelled results when comparing with the effects found by statistical data analysis in Sect. 3.

3 Statistical data analysis

To study whether the modelled effect is seen in real experiments, we have analysed IRIS absorption data from all beams shown in Fig. 1 for selected EISCAT heating experiments during 1994–2004.

Fig. 6. Dates of selected IRIS data 1994–2004.

Table 1. Heater configurations used during the selected experiments 1994–2004, percentages out of 18417 on/off modulations.

| Heater frequency (MHz)	Antenna field 1		Antenna field 2	
	o-mode	x-mode	o-mode	x-mode
4.0400	–	–	6.38%	19.4%
4.1000	–	–	0.05%	0.35%
4.5400	–	–	0.05%	–
4.5440	2.52%	–	0.57%	15.7%
4.9128	–	–	2.95%	–
5.3430	2.77%	–	–	–
5.3830	2.34%	–	–	–
5.4230	12.7%	13.8%	3.90%	0.39%
5.4400	–	–	0.07%	–
5.4700	–	–	0.34%	–
5.5000	–	1.00%	0.30%	-
5.6230	–	0.07%	–	–
6.2000	3.88%	0.90%	0.11%	-
6.7700	–	–	0.30%	–
6.8000	1.14%	–	–	–
7.1000	0.23%	0.21%	2.82%	–
7.9530	2.81%	1.00%	–	–
8.0800	–	0.86%	–	–
Total	28.4%	17.8%	17.9%	35.9%
	46.2%		53.8%	

3.1 Data selection

Data from vertical-beam heating experiments with simple on/off modulation and on/off times from 1 s (the IRIS time resolution) to 60 s were chosen. Imposing the latter restriction we avoid large natural background fluctuations during the modulations. These data, covering in total 18417 on/off modulations, represent all seasons, as shown in Fig. 6. The heater parameters used in these experiments are summarised in Table 1.

3.2 Absorption differences

As a basis for the statistical treatment of the absorption data we define an absorption difference for each on/off-modulation period as the difference between the mean absorption during the heater-on period and the mean absorption during the following heater-off period. If the absorption of cosmic radio noise is enhanced due to the heating, as theoretically predicted, the distribution of the absorption differences should have a positive offset for the overlapping beam (beam 9) as compared with the other beams. In Fig. 7 the left plot shows histograms of the background absorption and the right plot shows histograms of absorption differences for all selected experiments. The background absorption, defined as the mean absorption during each on/off-modulation, is classified into "low", "medium" and "high" as a measure of electron density. The limits are chosen so that one third of the data points fall into each category and this classification

is subsequently used for sorting the corresponding absorption differences in the following statistical analysis. Note that the "low" background absorption category contains many points of negative absorption. These do not necessarily represent low electron densities but are more likely the result of radio sources not properly included in the quiet-day curve.

In the right plot of Fig. 7 we see that the natural variation of the absorption differences is larger than the majority of the modelled differences shown in Fig. 4.

3.3 Bootstrap median error analysis

To find the possibly very small statistical offset of the absorption differences we use median estimates rather than averages because of their robustness in the presence of outliers. To quantify the accuracy of the median estimates without making any assumptions of the statistical distribution of the data, a Monte-Carlo method called bootstrap analysis (Efron, 1979) is used. In this approach it is assumed that the studied samples represent the statistical properties of the system well, so that any random subset of the original samples has the same statistical properties. It is then possible to obtain estimates for many subsets containing the same number of points as the original data, and hence to study the variance of the estimates in cases of different weightings of the original data.
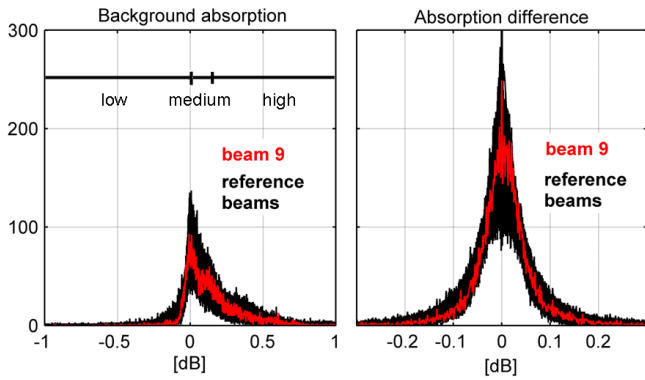
Fig. 7. Left panel: Histogram of background absorption (relative to quiet-day curve) during all selected heating experiments. Lines show the classification into low, medium and high background absorption cases, with one third of the points in each category. Right panel: Histograms of calculated absorption differences for IRIS beam 9 and the reference beams (all beams except no. 9) for these experiments.

We performed the bootstrap median estimates for 10 000 random subsets of the original data and of the data sorted according to heater antenna field and background absorption. Figure 8 shows these estimates for the 12 combinations of heater experiments (all, field 1, field 2) and backgrounds (all, low, medium, high). Error bars show the 95% confidence intervals, i.e., 9500 out of the 10 000 median estimates for each beam and criterion of data selection are within the shown limits. The results show a consistent offset in beam 9, except for the combinations of field 1 and low background absorption and possibly also field 2 with medium and high background absorption, for which the data points are too few to yield significant estimates.

Since the overlapping beam number 9 is the only one where the offset is always positive, we are confident that the difference is a result of the EISCAT heating experiments, even though the magnitude of the effect is very small. In fact, the effect is smaller than the digital quantisation of the IRIS A/D converter. However, this is not a limit for the resolution of the estimates shown in Fig. 8, because these are based on medians of many data points with a reasonable natural variance. It can be concluded that the median absorption enhancement is 0.002–0.005 dB.

4 Discussion

The input parameter sets used in our 24 modelling cases are chosen to represent the variety of typical conditions and heater parameters. The most typical experiment condition is a combination of winter time, medium electron density, antenna field 2 and heater x-mode, which gives an absorption difference of 0.02 dB. An effect of this magnitude is still
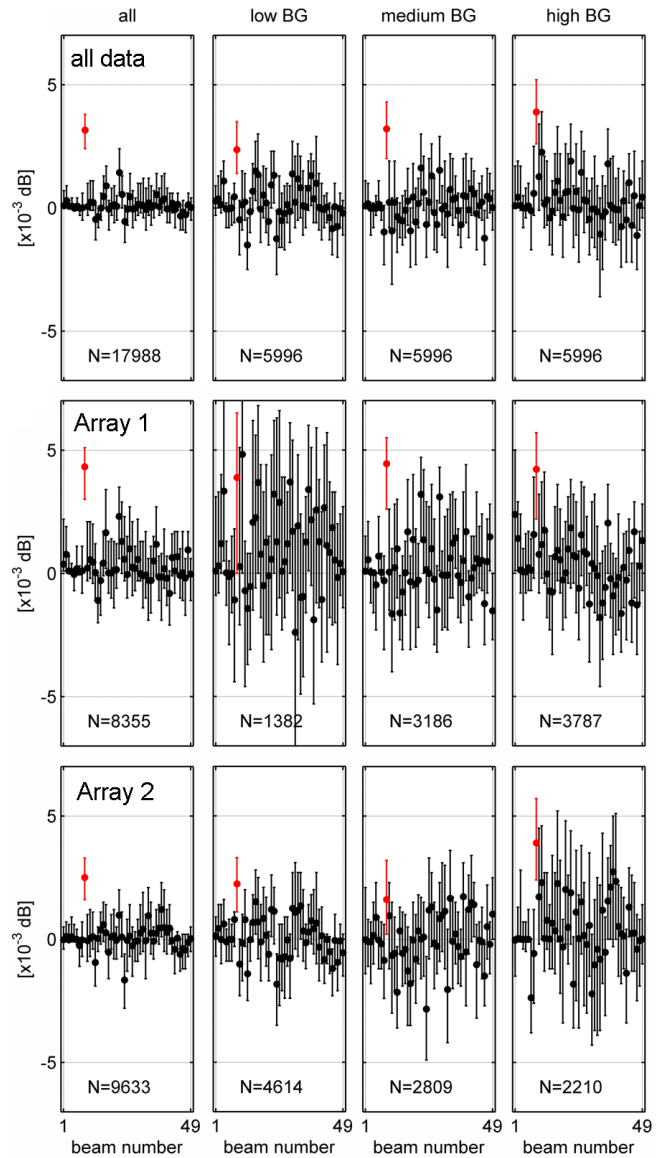
Fig. 8. Medians of the observed absorption differences, with 95% bootstrap error bars, for all IRIS beams. Beam 9 is shown in red. Upper line: All selected experiments. Middle line: EISCAT Heater antenna field 1 experiments. Lower line: Antenna field 2 experiments. Leftmost column: All data. Other columns: Selected data from the three categories of background absorption.

small compared with the background variation (see Fig. 7), but would be detectable even within single heating experiments. Moreover, in most of the modelled cases, especially in those experiments using antenna field 1, the effect should be higher, up to 0.07 dB at a maximum. The sensitivity studies in Sect. 2.5 show that the modelled results are robust to variation of heater frequency and also to all conceivable inaccuracies of IRIS beam directions. We have also verified that the spatial resolution ($N=401$) used in the modellings describes the geometry of the experiment sufficiently well.

The statistical analysis shows, however, that the effect in reality is very small. Large data sets containing data from the entire period 1994–2004 were necessary to discriminate the unique offset compared with the 48 reference beams at a 95% significance level. The median effect, representing the expectation value of the absorption difference, was found to be 0.002–0.005 dB. The effect was not unambiguously detectable in any single heating experiment in the data set.

In spite of the discrepancy, a factor of 5 to 10, it can be seen (comparing Figs. 4 and 8) that the model reproduces two significant features found in the statistical data analysis. Firstly, antenna field 1 produces approximately twice the absorption differences of field 2. Secondly, the absorption difference increases as a function of electron density (or background absorption).

To reproduce the measurements quantitatively a model scaling factor $k < 0.2$ is required. The reason for this discrepancy remains an open question. A large overestimate of the heater antenna gains would be a sufficient explanation, but the error is unlikely to be more than 1 dB and hence cannot account for this scaling factor (which would correspond to an overestimate of 7 dB). The remaining possibilities are that either

1. the energy production, as given by the imaginary part of the refractive index of Sen and Wyller (1960), is overestimated because the theory does not hold true for the collisional, almost neutral gas of the D-region, or

2. the loss rate of electron energy is in reality 5 to 10 times higher than in the model.

5   Conclusions

For the first time the D-region heating-induced enhancement of cosmic noise absorption has been quantified by determining the statistical enhancement of Kilpisjärvi IRIS absorption during EISCAT heating experiments. The expectation value of the effect during typical conditions is close to 0.003 dB. A rigorous 3-D modelling yields absorption differences between 0.02 dB and 0.07 dB.

Based on sensitivity studies we conclude that the discrepancy is not likely caused by any reasonable inaccuracies of the model input parameters. The reason remains an open question. Possibly the generalised magnetoionic theory of Sen and Wyller (1960) overestimates the production term (wave absorption), or there are additional electron energy loss processes not accounted for in our model.

References

Banks, P. and Kockarts, G.: Aeronomy, Academic Press Inc., 1973.

Belova, E. G., Pashin, A. B., and Lyatsky, W. B.: Passage of a powerful HF radio wave through the lower ionosphere as a function of initial electron density profiles, J. Atmos. Terr. Phys., 57, 265–272, 1995.

Browne, S., Hargreaves, J. K., and Honary, B.: An Imaging Riometer for Ionospheric Studies, Electronics and Communication Engineering Journal, 7, 209–217, 1995.

Detrick, D. L. and Rosenberg, T. J.: A Phased-Array Radiowave Imager for Studies of Cosmic Noise Absorption, Radio Sci., 25, 325–338, 1990.

Efron, B.: Bootstrap Methods. Another Look at the Jackknife., Annals of Statistics, 7, 1–26, 1979.

Enell, C.-F., Kero, A., Turunen, E., Ulich, T., Verronen, P. T., Seppälä, A., Marple, S., Honary, F., and Senior, A.: Effects of D-region RF heating studied by the Sodankylä Ion Chemistry model, Ann. Geophys., 23, 1575–1583, 2005, http://www.ann-geophys.net/23/1575/2005/.

Friedrich, M., Harrich, M., Torkar, K. M., and Kirkwood, S.: The disturbed auroral ionosphere based on EISCAT and rocket data, Adv. Space Res., 33, 949–955, 2004.

Hedin, A. E.: Extension of the MSIS Thermospheric Model into the Middle and Lower Atmosphere, J. Geophys. Res., 96, 1159–1172, 1991.

Honary, F. H., Marple, S., and Kavanagh, A.: Heater-induced Scintillation, in: 20th Anniversary Symposium on Ionospheric Interactions in Tromsø, EISCAT Scientific Association, Ramfjordmoen, Norway, 2000.

Kero, A., Bösinger, T., Pollari, P., Turunen, E., and Rietveld, M.: First EISCAT measurement of electron-gas temperature in the artificially heated D-region ionosphere, Ann. Geophys., 18, 1210–15, 2000, http://www.ann-geophys.net/18/1210/2000/.

Pashin, A. B., Kotikov, A. L., and Pudovkin, M. I.: Numerical simulation of auroral absorption in the artificially disturbed ionosphere, Geomagnetism and Aeronomy, 43, 59–62, 2003.

Pavlov, A. V.: New electron energy transfer rates for vibrational excitation of N_2, Ann. Geophys., 16, 176–182, 1998a.

Pavlov, A. V.: The role of vibrationally excited oxygen and nitrogen in the ionosphere during the undisturbed and geomagnetic storm period of 6–12 April 1990, Ann. Geophys., 16, 589–601, 1998b.

Rietveld, M. T., Kopka, H., and Stubbe, P.: D-region characteristics deduced from pulsed ionospheric heating under auroral electrojet conditions, J. Atmos. Terr. Phys., 48, 311–326, 1986.

Rietveld, M. T., Kohl, H., Kopka, H., and Stubbe, P.: Introduction to ionospheric heating at Tromsø-I. Experimental overview, J. Atmos. Terr. Phys., 55, 577–599, 1992.

Sen, H. K. and Wyller, A. A.: On the Generalization of the Appleton-Hartree Magnetoionic Formulas, J. Geophys. Res., 65, 3931–3950, 1960.

Stubbe, P. and Varnum, W. S.: Electron energy transfer rates in the ionosphere, Planet. Space Sci., 20, 1121–+, 1972.